Multi-channel conduction in redox-based resistive switch modelled using quantum point contact theory

E. Miranda,[1,a)] A. Mehonic,[2] J. Suñé,[1] and A. J. Kenyon[2]
[1]*Departament d'Enginyeria Electrònica, Universitat Autònoma de Barcelona, 08193 Cerdanyola del Vallés, Barcelona, Spain*
[2]*Department of Electronic and Electrical Engineering, University College London, Torrington Place, London WC1E 7JE, United Kingdom*

(Received 23 September 2013; accepted 12 November 2013; published online 27 November 2013)

A simple analytic model for the electron transport through filamentary-type structures in Si-rich silica (SiO_x)-based resistive switches is proposed. The model is based on a mesoscopic description and is able to account for the linear and nonlinear components of conductance that arise from both fully and partially formed conductive channels spanning the dielectric film. Channels are represented by arrays of identical scatterers whose number and quantum transmission properties determine the current magnitude in the low and high resistance states. We show that the proposed model not only reproduces the experimental current-voltage (I-V) characteristics but also the normalized differential conductance ($d\ln(I)/d\ln(V)$-V) curves of devices under test. © *2013 AIP Publishing LLC*. [http://dx.doi.org/10.1063/1.4836935]

Reversible dielectric breakdown occurring in oxide films under the application of ramped or pulsed voltages is currently considered as a feasible alternative for information storage cells in non-volatile memory devices.[1] A wide variety of binary oxides such as HfO_2,[2] TiO_2,[3] ZnO,[4] NiO,[5] and suboxides including TaO_x,[6] HfO_x,[7] NiO_x,[8] and SiO_x,[9] exhibit this property, which is expected to overcome the limits of scalability and power dissipation of current memory devices involving charge transfer or phase change mechanisms.[10] Among these materials, silicon-rich silica (SiO_x) has recently attracted a lot of attention because of its compatibility with standard CMOS technology.[9,11] The resistive switching (RS) effect in such oxides is often associated with the formation and dissolution of nanometre-scale conductive filaments bridging the dielectric film.[12] The presence of a conductive filament leads to a low resistance state (LRS), while the absence results in a high resistance state (HRS). The movement of oxygen vacancies and/or local Joule heating effects caused by the external applied potential drives the switching process.[1,13] In addition, several reports[14–17] have pointed out that the filaments exhibit conductance values close to the quantum conductance unit $G_0 = 2e^2/h$, where e is the electron charge and h is the Planck's constant. This is a well-known feature of atomic-sized constrictions.[18]

We showed in a recent paper[19] that the conduction characteristics of SiO_x-based resistive switches can be written as $I(V) = NG_0V + f(V)$, where N is an integer or half-integer number and $f(V)$ is a nonlinear function of the applied voltage. While we attributed the constant conductance term to a highly conductive filament core (see Fig. 1(a)), we assigned $f(V)$ to electron transport through a region around the core in which the conductive channel has not fully formed (see Fig. 1(b)). In this Letter, we develop an expression for $f(V)$ consistent with these ideas with the support of further experimental results. To this end, metal-insulator-metal structures were fabricated as follows: Si wafers with a pre-processed thermal 40 μm-thick SiO_2 layer were used as the substrate. The bottom electrode of the devices consisted of a uniform layer 100 nm-thick of TiN deposited by sputtering at room temperature. The SiO_x layers (30 nm thick) were deposited by magnetron cosputtering at 250 °C using two confocal cathodes: SiO_2 and Si under a pure Ar plasma. The excess silicon content of the films was 11 at. %. Samples were annealed at 600 °C post deposition in an Ar atmosphere. A top layer of TiN, identical to the one used for the bottom electrode, was deposited to form the top contacts, which were defined using standard lift-off techniques. The devices were initially electroformed with a maximum voltage ramp to around 7–8 V. The subsequent unipolar set process was typically a single abrupt jump in current at voltages around 3–4 V. As described in our previous work,[19] during electroforming, a conductive filament is produced inside the insulating film via local redox processes, and during the switching process, only a small fraction of the filament is changing. In all cases, the top electrode was positively biased during the unipolar set/reset processes. Because of the current compliance limit (10^{-3} A) used for the set process, in this paper, attention will be exclusively focused on the reset process, which includes both the LRS and HRS I-Vs.

Using the finite-bias Landauer approach for mesoscopic systems[18] and the additive property of the transmission probability for a series combination of identical scatterers,[20] the current that flows through a multichannel conductive structure can be expressed as

$$I(V) = \frac{2e}{h}\sum_i \int_{-\infty}^{\infty} \frac{[f(E - eV_i/2) - f(E + eV_i/2)]}{1 + S_i[(1 - t(E))/t(E)]} dE, \quad (1)$$

where the sum runs over the total number of channels that constitute the filament; E is the energy; f is the Fermi function; S_i the number of scatterers along the channel i; V_i is the voltage drop across the channel i, and $t(E)$ is the transmission probability for an individual scatterer. In our picture, which

a)Author to whom correspondence should be addressed. Electronic mail: enrique.miranda@uab.cat

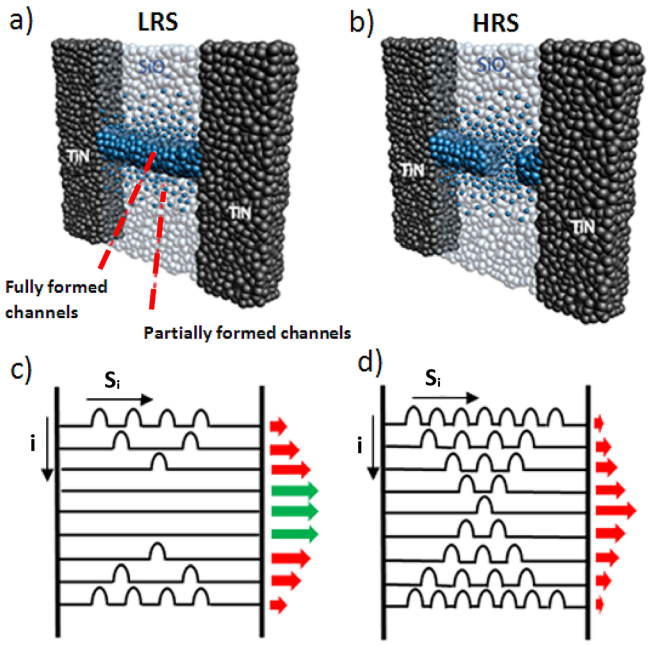

FIG. 1. (a) Schematic showing a filamentary leakage current path in the LRS of the device composed of fully (core region) and partially (cloud of defects or vacancies) formed channels. (b) Schematic showing a break in the filament within the oxide matrix, corresponding to the HRS of the device. (c) and (d) Arrangement of scatterers along the electron transport channels associated with cases (a) and (b), respectively. The green and red arrows represent the transmission probability of fully and partially formed channels, respectively. S_i is the number of scatterers along the channel i.

simulates the filament as a bunch of monomode nanowires, two types of channels coexist: fully and partially formed (see Figs. 1(c) and 1(d)). By a fully formed channel, we mean a perfectly transparent ($t(E)=1$) conduction channel with $S_i=0$, whereas by a partially formed channel, we mean a nanosized bridge with $S_i>0$ and $t(E)<1$. This approach is also compatible with the presence of isolated channels located far from the main constriction since no specific requirement about the spatial arrangement of the current pathways is made. Note that in Eq. (1), the current is calculated assuming that the applied bias is symmetrically distributed at both sides of the constriction, but asymmetrical conduction structures can be modeled as well.[21] For simplicity, it is also assumed that the phase-relaxation length is much shorter than the distance between the scatterers.[20,22] This means that interference effects between scatterers are completely neglected. Similar one-dimensional filamentary structures with scatterers have been the subject of numerous publications in the past.[23–28] Since we are looking for a mathematically tractable expression for the current, the scatterers are assumed to be described by inverted parabolic barriers of height Φ_0. These parabolic barriers could represent the potential bottlenecks between two neighbor atoms. In this case, $t(E)$ reads

$$t(E) = \{1 + \exp[-\alpha(E - \Phi_0)]\}^{-1}, \tag{2}$$

where α is a constant related to the longitudinal shape of the barrier.[29] Equation (1) can be easily integrated in the zero-temperature limit so as to give the approximate expression

$$I \approx G_0 \left[NV + \frac{2}{e\alpha} \exp(-\alpha\Phi_{eff}) \sinh\left(\frac{e\alpha V}{2}\right) \right], \tag{3}$$

where N is the number of formed channels. The effective barrier height Φ_{eff} in Eq. (3) is given by the expression

$$\Phi_{eff} = \Phi_0 - \ln\left(\sum_i S_i^{-1}\right)^{1/\alpha}. \tag{4}$$

We call $\Gamma = \sum_i S_i^{-1}$ the configuration factor of the constriction, which reflects the particular arrangement of scatterers that constitute the filament. As a very simplistic view of the problem, the first term of Eq. (3) is associated with the core of the constriction (LRS), whereas the second term, which we identify with $f(V)$, corresponds to the current flowing through the cloud of partially formed filaments surrounding the central region (HRS).[19] According to expression (3), in the absence of a core region (see Fig. 1(d)), the gap in the constriction can be represented by a single scatterer with an effective barrier Φ_{eff}, which simplifies the conduction problem enormously. As expected, expression (4) reveals that, while the presence of scatterers diminishes the current flow by increasing the potential barrier height, the generation of parallel current paths acts in the opposite manner. Figure 2 illustrates some fitting results using Eq. (3) for three typical I-V characteristics. Notice that log-linear and log-log axes have been used to highlight the agreement and deviation of the experimental data from the theoretical model. Remarkably, Γ is necessary to justify the low effective barrier heights used in Eq. (3), which otherwise would be incompatible with a tunnelling process. For the sake of simplicity, we consider a constant value $\Phi_0 = 1\,\text{eV}$ and neglect its statistical spread.[17,30] In Fig. 2, the conduction characteristic for a monomode ballistic conductor $I = G_0 V$ has been included for comparison. Figure 3 shows several hysteretic I-V loops ($0\,\text{V} \rightarrow V_{MAX} \rightarrow 0\,\text{V}$ with increased maximum voltage V_{MAX} from 1 V to 1.5 V). Contrary to what is observed in Fig. 2, no jumps are detected in the I-V curve, which indicates the progressive generation of new scatterers or, equivalently, the modification of Φ_{eff}. As proposed in Ref. 31, the dynamic behavior of Φ_{eff} as a function of the applied voltage determines the transition from HRS to LRS and vice-versa. The model described here makes no reference to this issue but $\Phi_{eff}(V)$ can be incorporated into the model as a coupled equation as is done for memristive systems.[32]

In order to achieve further insight into the electron transport mechanism proposed above, let us discuss in detail the nonlinear term in Eq. (3). According to this framework, the conductance of an individual scatterer, g_S, can be calculated as[20]

$$g_s(E) = G_0 \frac{t(E)}{1 - t(E)} = g_s^0 \exp[\alpha E], \tag{5}$$

where $g_s^0 = g_s(E=0) = G_0 \exp(-\alpha\Phi_0)$ is the conductance at the equilibrium energy $E=0$. Hence, the conductance of the constriction G_C which arises from the bunch of partially formed channels, can be written as

$$G_C(E) = \sum_i \left(\sum {g_s}^{-1}(E)\right)^{-1} = g_s^0 \Gamma \exp(\alpha E). \tag{6}$$

Expression (6) stems from the scatterers in series and the additive property of the transmission probability already

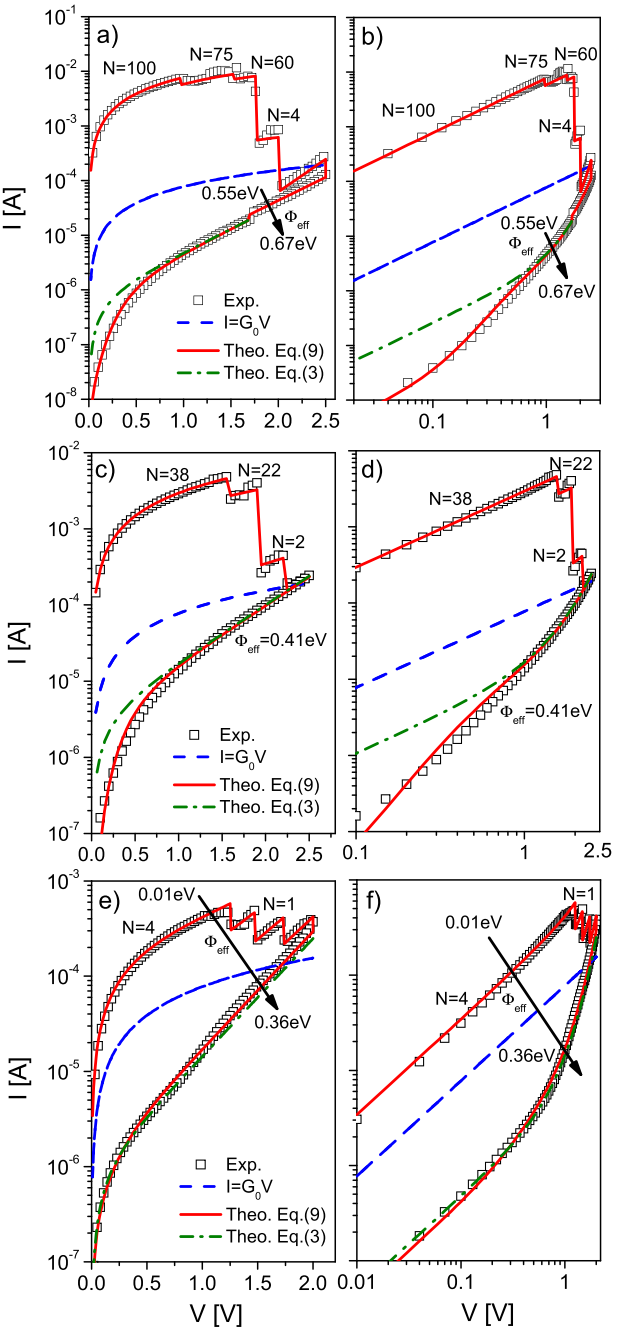

FIG. 2. Typical current-voltage characteristics with multiple reset events. The curves exhibit different behavior at low biases, which are attributed to particular features of the filaments. N is the number of formed channels and Φ_{eff} is the effective barrier height in Eqs. (3) and (9). The symbols are experimental data; the red solid line corresponds to the model using Eq. (9), while the green dotted-dashed line was calculated using Eq. (3). The blue dashed line is the I-V characteristic for a monomode ballistic conductor.

used in Eq. (1). Consequently, the average conductance of the constriction $\langle G_C \rangle$ reads

$$\langle G_C(V) \rangle = \frac{1}{eV} \int_{-eV/2}^{+eV/2} G_C(E) dE = G_0 \exp(-\alpha \Phi_{eff}) \mathrm{sinhc}\left(\frac{e\alpha}{2} V\right), \tag{7}$$

where the function sinhc(x) is defined as $\sinh(x)/x$. Substituting Eq. (7) into Eq. (3) and taking into account the N formed channels, we obtain

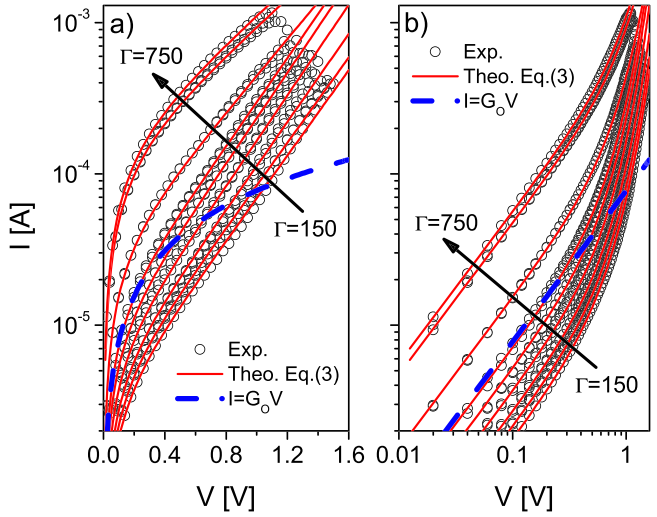

FIG. 3. Typical hysteretic current-voltage characteristics without abrupt jumps. The symbols are experimental data; the red solid line corresponds to the model using Eq. (3). The blue dashed line is the I-V characteristic for a monomode ballistic conductor. Γ is the constriction configuration factor.

$$I(V) = (NG_0 + \langle G_C \rangle)V, \tag{8}$$

which expresses the total current as a combination of the core current contribution and that associated with the nearby cloud of scatterers. Notice that as the scatterers become transparent ($\alpha \ll 1$ in Eq. (7)), $\langle G_C \rangle \approx \Gamma G_0$ is a constant and the linear behavior of the I-V curve is recovered. Remarkably, even though Eq. (3) can be formally rearranged as Eq. (8) without invoking $\langle G_C \rangle$, the latest formulation did not include the contact conductances, as Eq. (3) implicitly does, and which arise from the mismatch of the energy states occurring at the connections between the metal reservoirs and the channels.[20] This coincidence is a consequence of the approximation $t(E) \approx S_i^{-1} \exp[\alpha(E - \Phi_0)]$ used to obtain Eq. (3).

In order to improve the fitting results in the HRS low-bias region (see Figs. 2(a)–2(d)), the correction factor $V_0(V) = A\tanh(BV)$ can be introduced into Eq. (3) as

$$I \approx G_0 \left\{ NV + \frac{2}{e\alpha} \exp(-\alpha \Phi_{eff}) \sinh\left[\frac{e\alpha}{2}(V - V_0(V))\right] \right\}, \tag{9}$$

where A and B are fitting constants. Note that this additional potential drop V_0 is not required for the formed channels. A similar expression for the effective potential drop has been used before in other RS devices to deal with the semiconducting behavior of the bottom electrode.[33] A dependence of the effective barrier height on the applied voltage cannot be ruled out. Expression (9) is chosen this way because it satisfies $V_0(V = 0) = 0$; $V_0(V \ll 1)$ is a linear function of V, and $V_0(V \gg 1)$ is a constant which does not affect the exponential dependence of the HRS current in the high-bias range. The fact that V_0 is unnecessary to fit some HRS I-Vs (see Figs. 2(e), 2(f), 3(a), and 3(b)) indicates that the faster roll-off of the experimental current for $V < 1$ V is related to particular features of the filaments and not to an essential limitation of the model. Notice that if Eq. (9) is used, a lower Φ_{eff} is required to compensate for the lower effective applied bias.

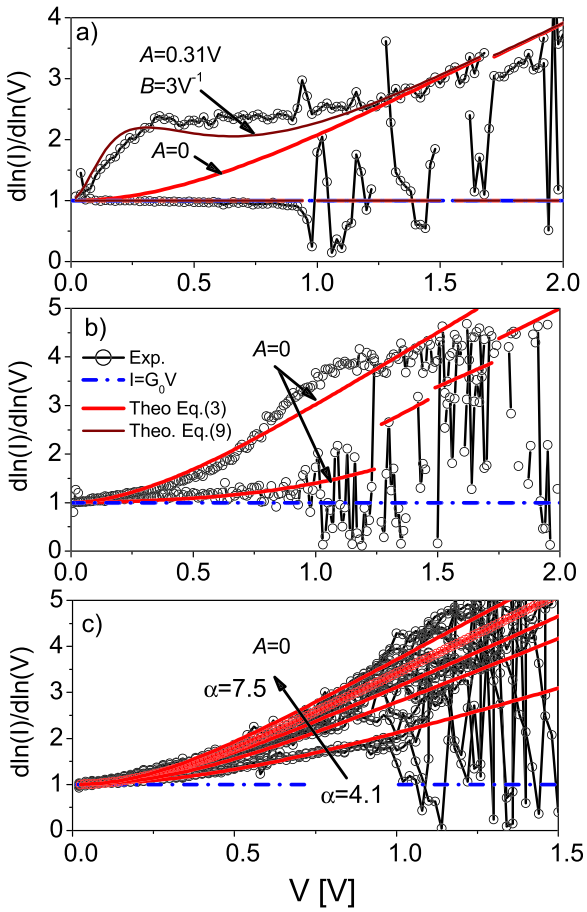

FIG. 4. Normalized differential conductance-voltage characteristics for three cases of particular interest: (a) corresponds to the *I-V* curve shown in Fig. 2(c), (b) corresponds to the *I-V* curve shown in Fig. 2(e), and (c) corresponds to the I-V curves shown in Fig. 3(a). Notice that the correction factor V_0 (Eq. (9)) is only used in the first case. The blue dashed line is the *g-V* characteristic for a monomode ballistic conductor.

Finally, with the aim of analyzing in more detail the experimental *I-V* curves, the normalized differential conductance *g(V)* is used. For the two limiting cases we are dealing with, using Eq. (3), *g(V)* reads

$$g(V) = \frac{d\ln I}{d\ln V} = \frac{V}{I}\frac{dI}{dV} = \begin{cases} 1 & N \gg 1 \\ \frac{\alpha e}{2} V \coth\left(\frac{\alpha e}{2} V\right) & N = 0 \end{cases}, \quad (10)$$

which is independent of Φ_{eff}, and therefore of Γ. In this way, we were able to eliminate one model parameter. This is illustrated in Fig. 4 for three cases of particular interest: Figs. 4(a)–4(c) correspond to Figs. 2(c), 2(e), and 3(a), respectively. In Fig. 4(a), the obtained results using Eqs. (3) and (9) are compared. In Fig. 4(b), departures from $g(V) \approx 1$ in the LRS case would indicate the presence of a nonlinear conductance term. In Fig. 4(c), the set of *I-V* hysteretic loops is represented. The only free parameter is α. Notice also that in all the cases $g(V \ll 1) \approx 1$, regardless of the conduction mode. This linear behavior of the *I-V* characteristic at low voltages is a well-known feature of RS devices[4] that our model captures nicely.

In summary, we report a simple analytic model for the *I-V* characteristics of SiO_x-based resistive switching devices. The model relies on the theory of mesoscopic conductors and considers the filamentary electron transport pathways within the dielectric film as chains of scatterers whose transmission properties collectively determine not only the magnitude of the current (low and high resistance states) but also its functional dependence on the applied voltage (linear or exponential). The stochastic nature of the atomic arrangement that forms the constriction (configuration factor) is overridden by assuming an effective tunneling barrier.

This work was funded in part by the Spanish Ministry of Science and Technology under Contract No. TEC2012-32305 and the DURSI of the Generalitat de Catalunya under Contract No. 2009SGR783. A.J.K and A.M are grateful for financial support from the Engineering and Physical Sciences Research Council under Grant No. EPK01739X/1. E. Miranda acknowledges the Royal Academy of Engineering, United Kingdom for a Distinguished Visiting Fellowship Award 2013.

[1]R. Waser, R. Dittmanm, G. Stakov, and K. Szot, Adv. Mater. **21**, 2632 (2009).
[2]Y. Chen, G. Pourtois, C. Adelmann, L. Goux, B. Govoreanu, R. Degraeve, M. Jurczak, J. Kittl, G. Groeseneken, and D. Wouters, Appl. Phys. Lett. **100**, 113513 (2012).
[3]K. Kim, G. Kim, S. Song, J. Seok, M. Lee, J. Yoon, and C. Seong Hwang, Nanotechnology **21**, 305203 (2010).
[4]S. Lee, H. Kim, D. Yun, S. Rhee, and K. Yong, Appl. Phys. Lett. **95**, 262113 (2009).
[5]Q. Sun, J. Gu, L. Chen, P. Zhou, P. Wang, S. Ding, and D. Zhang, IEEE Electron Device Lett. **32**, 1167 (2011).
[6]J. Joshua Yang, M. Zhang, J. Strachan, F. Miao, M. Pickett, R. Kelley, G. Medeiros-Ribeiro, and R. Stanley Williams, Appl. Phys. Lett. **97**, 232102 (2010).
[7]D. Ielmini, Tech. Dig. - Int. Electron Device Meet. **2011**, 17.2.1.
[8]K. Kinoshita, T. Tamura, M. Aoki, Y. Sugiyama, and H. Tanaka, Appl. Phys. Lett. **89**, 103509 (2006).
[9]A. Mehonic, S. Cueff, M. Wojdak, S. Hudziak, O. Jambois, C. Labbé, B. Garrido, R. Rizk, and A. J. Kenyon, J. Appl. Phys. **111**, 074507 (2012).
[10]V. Zhirnov, R. Meade, R. Cavin, and G. Sandhu, Nanotechnology **22**, 254027 (2011).
[11]L. Zhang, R. Huang, D. Gao, D. Wu, Y. Kuang, P. Tang, W. Ding, A. Wang, and Y. Wang, IEEE Electron Device Lett. **30**, 870 (2009).
[12]K. Kim, D. Jeong, and C. Hwang, Nanotechnology **22**, 254002 (2011).
[13]A. Sawa, Mater. Today **11**, 28 (2008).
[14]E. Miranda, C. Walczyk, C. Wenger, and T. Schroeder, IEEE Electron Device Lett. **31**, 609 (2010).
[15]X. Zhu, W. Su, Y. Liu, B. Hu, L. Pan, W. Lu, J. Zhang, and R. Li, Adv. Mater. **24**, 3941 (2012).
[16]R. Degraeve, P. Roussel, L. Goux, D. Wouters, J. Kittl, L. Altimime, M. Jurczak, and G. Groeseneken, in Proceedings of the International Meeting on Electron Devices (2010), p. 28.
[17]L. Prócel, L. Trojman, J. Moreno, F. Crupi, V. Maccaronio, R. Degreave, L. Goux, and E. Simoen, J. Appl. Phys. **114**, 074509 (2013).
[18]N. Agrait, A. Levy Yeyati, and J. van Ruitenbeek, Phys. Rep. **377**, 81 (2003).
[19]A. Mehonic, A. Vrajitoarea, S. Cueff, S. Hudziak, H. Howe, C. Labbé, R. Rizk, M. Pepper, and A. J. Kenyon, Sci. Rep. **3**, 2708 (2013).
[20]S. Datta, *Electronic Transport in Mesoscopic Systems* (Cambridge University Press, 1997).
[21]J. Pascual, J. Torres, and J. Sáenz, Phys. Rev. B **55**, R16029 (1997).
[22]S. Datta, *Quantum Transport: Atom to Transistor* (Cambridge University Press, New York, 2005).
[23]X. Wu, K. Li, N. Raghavan, M. Bosman, Q. Wang, D. Cha, X. Zhang, and K.-L. Pey, Appl. Phys. Lett. **99**, 093502 (2011).
[24]X. Liu, K. Biju, J. Lee, J. Park, S. Kim, S. Park, J. Shin, S. Sadaf, and H. Hwang, Appl. Phys. Lett. **99**, 113518 (2011).
[25]M. Sasaki, J. Appl. Phys. **112**, 014501 (2012).
[26]R. Borland, Proc. Phys. Soc. **77**, 705 (1961).
[27]E. Miranda and J. Suñé, IEEE Int. Reliab. Phys. Symp. Proc. **2011**, 367.

[28]M. Xu and C. Tan, Appl. Phys. Lett. **92**, 082905 (2008).
[29]K. Hansen and M. Brandbyge, J. Appl. Phys. **95**, 3582 (2004).
[30]X. Lian, E. Miranda, S. Long, L. Perniola, M. Liu, and J. Suñé, in Proceedings of the International Conference on Ultimate Integration on Silicon (2013), pp. 161–164.
[31]E. Miranda, D. Jiménez, and J. Suñé, IEEE Electron Device Lett. **33**, 1474 (2012).
[32]L. Chua, Appl. Phys. A **102**, 765 (2011).
[33]E. Miranda, S. Kano, C. Dou, K. Kakushima, J. Suñé, and H. Iwai, Appl. Phys. Lett. **101**, 012910 (2012).